

Floquet chiral magnetic effect

Sho Higashikawa¹, Masaya Nakagawa², and Masahito Ueda^{1,2}

¹ *Department of Physics, University of Tokyo, 7-3-1 Hongo, Bunkyo-ku, Tokyo 113-0033, Japan*

² *RIKEN Center for Emergent Matter Science (CEMS), Wako, Saitama 351-0198, Japan*

(Dated: March 1, 2022)

A single Weyl fermion, which is prohibited in static lattice systems by the Nielsen-Ninomiya theorem, is shown to be realized in a periodically driven three-dimensional lattice system with a topologically nontrivial Floquet unitary operator, manifesting the chiral magnetic effect. We give a topological classification of Floquet unitary operators in the Altland-Zirnbauer symmetry classes for all dimensions, and use it to predict that all gapless surface states of topological insulators and superconductors can emerge in bulk quasienergy spectra in Floquet systems.

In 1981, Nielsen and Ninomiya proved that a single Weyl fermion cannot be realized in lattice systems [1, 2]. This theorem places a fundamental constraint on band structures due to the topology of the Brillouin zone. Weyl fermions have recently played a key role in cross-fertilizing ideas from high-energy physics and condensed-matter physics. A prime example is the predictions of Weyl semimetals [3, 4], where the low-energy effective field theory of Weyl fermions predicts novel electromagnetic responses originating from the chiral anomaly [5–8]. In particular, the observations of the surface Fermi arc [9–15] and anomalous transport [16–19] have aroused considerable interest. However, if a system is defined on a lattice and thus anomaly-free, the Nielsen-Ninomiya theorem dictates that a Weyl fermion be accompanied by its partner with opposite chirality. By the same token, an anomaly-induced response known as the chiral magnetic effect (CME) [20] does not occur in equilibrium [21], and numerous attempts to circumvent this difficulty have been made [22–28].

In this Letter, we demonstrate that a single Weyl fermion can be realized on a periodically driven lattice, thereby overcoming the above limitations. In periodically driven (Floquet) systems, the unitary time-evolution operator over one period defines an effective Hamiltonian and the associated quasienergies [29]. Despite the apparent similarity to static systems, Floquet systems enable realizations of exotic phases that cannot be reached in equilibrium, such as anomalous topological insulators [30, 31] and time crystals [32, 33]. The key idea of our proposal is an emerging topological structure in unitary operators associated with the periodicity of quasienergies [30]. We show that a driving protocol for a three-dimensional (3D) Thouless pump [30, 34] given by a topological Floquet unitary operation realizes a single Weyl fermion in a 3D lattice system, thereby providing a platform to observe the CME. We study the dynamics of a spin-polarized wave packet under our driving protocol and confirm that the fermion moves along its spin direction due to the spin-momentum locking of Weyl fermions. We demonstrate that a wave packet shows chiral transport under an applied synthetic magnetic field, leading to a Floquet realization of the CME. Our proposal can be implemented by using ultracold atomic gases, where the Thouless pump has been experimentally realized [35, 36].

Furthermore, we provide a topological classification of Floquet unitary operators in the Altland-Zirnbauer symmetry classes. In general, a wide variety of lattice-prohibited band structures under given symmetries can be realized as gapless surface states of topological phases [37]. The impossibility of pure lattice realization of surface states is deeply connected with their symmetry-protected gaplessness via quantum anomalies [38–40]. We show that the classification of topological Floquet unitaries, which generically offer symmetry-protected gapless quasienergy spectra, coincides with that of gapless surface states of static topological insulators/superconductors (TIs/TSCs). This correspondence strongly suggests that one can realize any gapless surface states of TIs/TSCs as *bulk* quasienergy bands of Floquet systems, even though they cannot be realized in static lattice systems.

Model.— We consider spin-1/2 fermions on a cubic lattice with a sublattice structure in the third direction. The lattice constant a is set to be unity: $a = 1$. The main ingredient of our model is spin-selective Thouless pumps [30, 34, 41] whose time evolution (unitary) operators U_j^\pm ($j = 1, 2, 3$) are given by

$$\begin{aligned} U_j^\pm &:= \sum_{\mathbf{x}} \sum_{\alpha, \beta = \uparrow, \downarrow} \left[(P_j^\pm)^{\alpha\beta} c_{\mathbf{x} \pm \mathbf{e}_j, \alpha}^\dagger c_{\mathbf{x}, \beta} + (P_j^\mp)^{\alpha\beta} c_{\mathbf{x}, \alpha}^\dagger c_{\mathbf{x}, \beta} \right] \\ &= \sum_{\mathbf{k}} c_{\mathbf{k}}^\dagger U_j^\pm(k_j) c_{\mathbf{k}}, \end{aligned} \quad (1)$$

where $\mathbf{x} = (x_1, x_2, x_3)$ and $\mathbf{k} = (k_1, k_2, k_3)$ denote the lattice site and the crystal momentum, respectively, \mathbf{e}_j is a unit vector in the x_j direction, and $c_{\mathbf{x}} = (c_{\mathbf{x}, \uparrow}, c_{\mathbf{x}, \downarrow})$ is the annihilation operator of a fermion with spin α (\uparrow or \downarrow) at site \mathbf{x} . The matrix $P_j^\pm := (\sigma_0 \pm \sigma_j)/2$ is a projection operator on a spin state $\sigma_j = \pm 1$, with σ_0 and σ_j ($j = 1, 2, 3$) being the 2×2 identity matrix and the Pauli matrices, and $U_j^\pm(k) := P_j^\pm e^{\mp i k_j} + P_j^\mp$. From the projective nature of P_j^\pm , under the pump U_j^\pm (U_j^-), fermions in a spin state $\sigma_j = +1$ (-1) are displaced by one lattice site in the positive (negative) x_j direction, while those in a spin state $\sigma_1 = -1$ ($+1$) are not, thereby achieving spin-selective transport (see Figs. 1 (a)-(d)). We also introduce spin-selective Thouless pump operators $U_{h,3}^\pm$ which displace

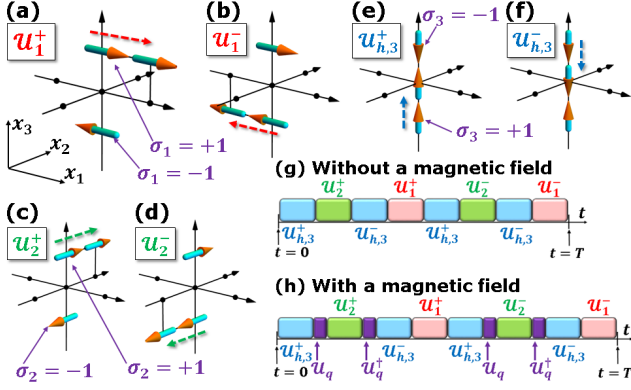


FIG. 1: (a)-(f): Schematic illustration of the fermion pump by U_j^\pm ($j = 1, 2$) and $U_{h,3}^\pm$ in Eqs. (1) and (2) in the 3D lattice with a sublattice structure in the third direction. Thick arrows show the spin directions of fermions, and thin dashed arrows show the direction of displacement. (g), (h): Driving protocols of the pump (g) without and (h) with a magnetic field. Here U_q is the time evolution operator induced by a sudden switch-on and -off of a quadrupole potential.

fermions by a half lattice site in the x_3 direction:

$$U_{h,3}^\pm := \sum_{\mathbf{k}} c_{\mathbf{k}}^\dagger U_{h,3}^\pm(k_3) c_{\mathbf{k}}, \quad (2)$$

where $U_{h,3}^\pm(k_3) = U_{\pm}^\pm(k_3/2)$ (see Figs. 1 (e) and (f)).

The driving protocol of our topological pump is constituted from eight successive applications of U_1^\pm , U_2^\pm , and $U_{h,3}^\pm$ as shown in Fig. 1 (g), where the total time evolution operator U_F over one cycle is (see Fig. 1 (g))

$$\begin{aligned} U_F &:= U_1^- U_{h,3}^- U_2^- U_{h,3}^+ U_1^+ U_{h,3}^- U_2^+ U_{h,3}^+ \\ &= \sum_{\mathbf{k}} c_{\mathbf{k}}^\dagger U(\mathbf{k}) c_{\mathbf{k}}. \end{aligned} \quad (3)$$

Then, the Floquet-Bloch operator $U(\mathbf{k})$ is given by

$$\begin{aligned} U(\mathbf{k}) &= U_1^-(k_1) U_{h,3}^-(k_3) U_2^-(k_2) U_{h,3}^+(k_3) \\ &\times U_1^+(k_1) U_{h,3}^-(k_3) U_2^+(k_2) U_{h,3}^+(k_3). \end{aligned} \quad (4)$$

A straightforward calculation shows that $U(\mathbf{k})$ stays constant if \mathbf{k} belongs to the boundary of the Brillouin zone $\mathbb{T}^3 := [-\pi, \pi]^3$ and hence satisfies the periodic boundary condition on \mathbb{T}^3 . This unitary $U(\mathbf{k})$ achieves a topologically nontrivial map from \mathbb{T}^3 to $SU(2) \cong S^3$ (3D sphere) with a unit winding number [42, 43]:

$$W := - \int \frac{d\mathbf{k}}{24\pi^2} \sum_{i,j,k=1}^3 \epsilon^{ijk} \text{Tr} [R_i R_j R_k] = 1, \quad (5)$$

where $R_i := U(\mathbf{k})^\dagger \partial_{k_i} U(\mathbf{k})$. This topological property is crucial for realizing a single Weyl fermion as detailed below.

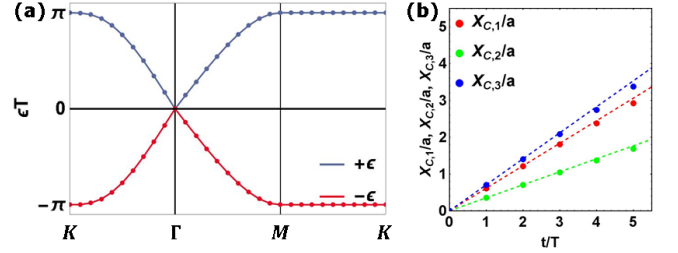


FIG. 2: Quasienergy spectra $\epsilon(\mathbf{k})$ (blue) and $-\epsilon(\mathbf{k})$ (red) along the loop connecting the points $K = (\pi, \pi, \pi)$, $M = (0, \pi, \pi)$, and $\Gamma = (0, 0, 0)$ within the Brillouin zone $\mathbb{T}^3 = \{(k_1, k_2, k_3) | -\pi \leq k_j \leq \pi\}$ of the cubic lattice. The quasienergy spectra extend over $-\pi \leq \epsilon(\mathbf{k}) \leq \pi$. (b) Time evolution of the center of mass \mathbf{X}_C of a wave packet, where the red, green, and blue points denotes the x_1 , x_2 , and x_3 components of \mathbf{X}_C . The initial state is a spin-polarized Gaussian wave packet with width $r_0 = 10$ and the spin polarization $\mathbf{S} = (\sqrt{6}/4, \sqrt{2}/4, \sqrt{2}/2)$. The numerical results (points) agree well with the theoretical curve $\mathbf{X}_C = t\mathbf{S}$ (dashed lines).

Dispersion and dynamics.— Let $h_{\text{eff}}(\mathbf{k})$ be an effective Hamiltonian defined by $U(\mathbf{k}) =: \exp[-ih_{\text{eff}}(\mathbf{k})]$, where the driving period T is set to be unity. Since the quasienergies $\epsilon(\mathbf{k})$ (eigenvalues of $h_{\text{eff}}(\mathbf{k})$) satisfy $\cos[\epsilon(\mathbf{k})] = \text{Tr}[U(\mathbf{k})]/2$, $\epsilon(\mathbf{k}) = \pm \cos^{-1}[2 \cos^2(\frac{k_1}{2}) \cos^2(\frac{k_2}{2}) \cos^2(\frac{k_3}{2}) - 1]$ follows from Eq. (4). The quasienergy spectrum along the loop connecting $\Gamma = (0, 0, 0)$, $M = (0, \pi, \pi)$, and $K = (\pi, \pi, \pi)$ is plotted in Fig. 2 (a). One can see that h_{eff} vanishes only at the Γ point, around which the dispersions are linear. Since $U(\mathbf{k})$ can be expanded around the Γ point as $U(\mathbf{k}) \approx \sigma_0 - i\mathbf{k} \cdot \boldsymbol{\sigma}$ from $U_j^\pm(k) \approx \sigma_0 \mp iP_j^\pm k$ for $k \approx 0$, the effective Hamiltonian can be written as $h_{\text{eff}}(\mathbf{k}) \approx \mathbf{k} \cdot \boldsymbol{\sigma}$, which clearly indicates the presence of a single left-handed Weyl fermion. We note that the quasienergies are constant between the M and K points, since we have $U(\mathbf{k}) = -\sigma_0$ on the boundary of \mathbb{T}^3 [44]. We also note that our model should be distinguished in topology from the previous proposals for realizing Floquet Weyl semimetals [45–54], where the Weyl nodes always appear in pairs in accordance with the Nielsen-Ninomiya theorem.

We now show that the dynamics under the driving protocol U_F reflects the spin-momentum locking of the Weyl fermions. To see this, consider a spin-polarized wave packet $\psi(\mathbf{k}, t = 0)$ localized at $\mathbf{k} = 0$ with width $\delta k \ll 2\pi$ and spin polarization \mathbf{S} . The wave packet $\psi(t)$ at time $t = nT$ is given by $\psi(nT) = (U_F)^n \psi(0)$, where the shift of the center of mass $\mathbf{X}_C := \int d\mathbf{x} \mathbf{x} |\psi(\mathbf{x}, t)|^2$ is calculated as $\mathbf{X}_C(t) \approx t\mathbf{S}$ [55]. We numerically solve the discrete-time Schrödinger equation $\psi(t+T) = U_F \psi(t)$ for the parameters $\delta k = 1/10$ and $\mathbf{S} = (\sqrt{6}/4, \sqrt{2}/4, \sqrt{2}/2)$. The time evolution of \mathbf{X}_C (points in Fig. 2 (b)) are in excellent agreement with the theoretical line $\mathbf{X}_C(t) = t\mathbf{S}$

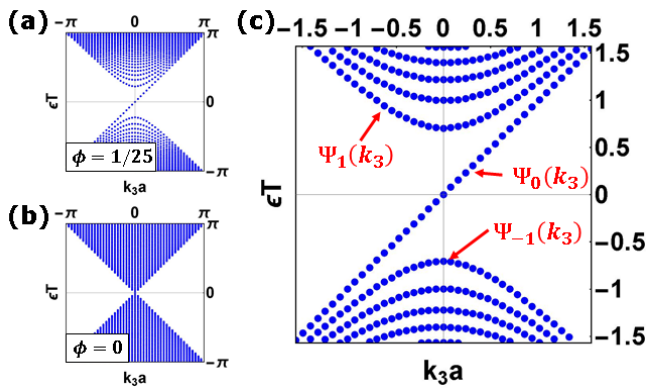


FIG. 3: (a), (b): Quasienergy spectra of $\bar{U}(k_2 = 0, k_3)$ with flux (a) $\phi = 1/25$ and (b) $\phi = 0$. (c): Quasienergy spectrum with $\phi = 1/25$ near the Weyl point at $k_3 = 0$. The three bands Ψ_1 , Ψ_0 , and Ψ_{-1} are the lowest particle band, the chiral band, and the highest hole band, respectively.

(dashed lines in Fig. 2 (b)).

Floquet chiral magnetic effect.— When a magnetic field is applied, a Weyl fermion shows chiral transport parallel to the applied magnetic field, a phenomenon known as the CME [20]. A magnetic field can be introduced in our model through the replacement of \mathcal{U}_2^\pm in Eq. (4) with $\mathcal{U}_q^\dagger \mathcal{U}_2^\pm \mathcal{U}_q$ (see Fig. 1 (h)), where $\mathcal{U}_q := \exp(-i2\pi\phi x_1 x_2)$ is the time evolution operator induced by a sudden switch-on and -off of a quadrupole potential [56]. Since $\mathcal{U}_q^\dagger \mathcal{U}_2^\pm \mathcal{U}_q = U_2^\pm(k_2 - 2\pi\phi x_1)$, the effective Hamiltonian near $\mathbf{k} = 0$ is given by $h_{\text{eff}} = (\mathbf{k} + \mathbf{A}) \cdot \boldsymbol{\sigma}$ with $\mathbf{A} = (0, -2\pi\phi x_1, 0)$, which describes a Weyl fermion under a magnetic field $\mathbf{B} = (0, 0, -2\pi\phi)$. Since k_2 and k_3 are good quantum numbers, the entire protocol \bar{U}_F is decomposed into a set of one-dimensional lattice models [57] as $\bar{U}_F = \sum_{k_2, k_3 \in [-\pi, \pi]^2} \bar{U}(k_2, k_3)$. Figure 3 (a) and (b) show the quasienergy spectra of $\bar{U}(0, k_3)$ for $\phi = 1/25$ and $\phi = 0$, respectively, and Fig. 3 (c) shows an enlarged spectrum near the Weyl point at $k_3 = 0$ for $\phi = 1/25$. Due to the flux ϕ , the Landau gap with size $2\omega := 4\sqrt{\pi\phi} \approx 1.4$ opens near the Weyl point, and a chiral dispersion emerges inside the gap.

Due to the chiral dispersion, a spin-polarized wave packet moves in the direction opposite to the applied magnetic field under the driving protocol \bar{U}_F , which is a Floquet realization of the CME. Let $l_B = 1/\sqrt{2\pi\phi}$ be the magnetic length. For clear demonstration of the Floquet CME, we initially prepare a spin-polarized Gaussian wave packet $\psi(\mathbf{x}, t = 0)$ with spin polarization \mathbf{S} and width $l_B (\gg 1)$ in the x_1 direction and $r_0 (\gg l_B)$ in the other directions (see the inset in Fig. 4), where $\psi(\mathbf{x}, t = 0) = \mathcal{N}^{-1/2} \exp[-\frac{(x_1)^2}{2(l_B)^2} - \frac{(x_2)^2 + (x_3)^2}{2(r_0)^2}] \mathbf{v}$ with $\sqrt{\mathcal{N}} = (\pi)^{3/2} (l_B)^{1/2} r_0$ and $\mathbf{S} = \langle \mathbf{v}, \boldsymbol{\sigma} \mathbf{v} \rangle$. Then, its Fourier transform $\psi(t = 0, k_2, k_3)$ is localized at $k_2 = k_3 = 0$ and can be expanded as $\psi(t =$

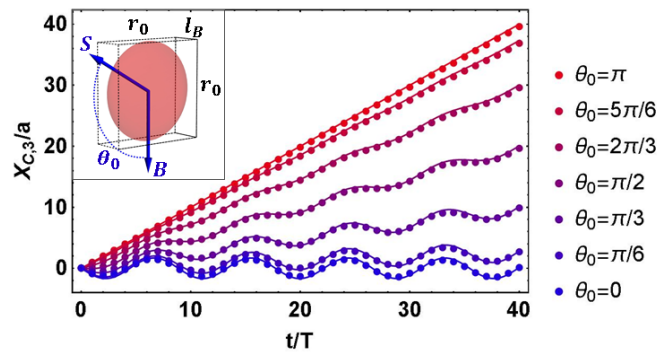


FIG. 4: Time evolution of the center of mass $X_{C,3}$ along the direction of the applied magnetic field $\mathbf{B} = (0, 0, -2\pi\phi)$ with $\phi = 1/25$ for relative angles $\theta_0 = 0$ (blue), $\pi/6, \pi/3, \pi/2, 2\pi/3, 5\pi/6, \pi$ (red). The solid curves are the theoretical ones in Eq. (6). The inset shows a schematic illustration of the initial pancake-shaped wave packet with widths l_B, r_0 , and r_0 in the x_1 -, x_2 -, and x_3 -directions, respectively, and θ_0 is the angle between \mathbf{B} and the spin polarization \mathbf{S} .

$0, k_2, k_3) \propto \sin\left(\frac{\theta_0}{2}\right) \Psi_0(k_3) + i \cos\left(\frac{\theta_0}{2}\right) \frac{\Psi_1(k_3) - \Psi_{-1}(k_3)}{\sqrt{2\omega}}$, where $\Psi_{-1}(k_3), \Psi_0(k_3)$, and $\Psi_1(k_3)$ are the lowest particle band, the chiral band, and the highest hole band of the Landau levels (see Fig. 3 (c)), respectively, and θ_0 is the angle between \mathbf{B} and \mathbf{S} . We numerically solve the discrete-time Schrödinger equation $\psi(t + T) = \bar{U}_F \psi(t)$ to calculate the time evolution of the shift $X_{C,3}(t) = \int d\mathbf{x} x_3 |\psi(\mathbf{x}, t)|^2$ in the center of mass parallel to $\mathbf{B} \parallel \mathbf{e}_3$. The results of $X_{C,3}(t)$ at the discrete times $t = 0, T, 2T, \dots$ for various θ_0 are shown as the points in Fig. 4. They are well fitted by the theoretical curve

$$X_{C,3}(t) = \sin^2\left(\frac{\theta_0}{2}\right) t - \frac{1}{2\omega} \cos^2\left(\frac{\theta_0}{2}\right) \sin(2\omega t), \quad (6)$$

which is derived from the Weyl equation in the continuous spacetime under a magnetic field [58]; $i\partial_t \psi = (\mathbf{k} + \mathbf{A}) \cdot \boldsymbol{\sigma} \psi$ with $\mathbf{A} = (0, -2\pi\phi x_1, 0)$. After a sufficiently long time $t \gg T$, the center of mass moves linearly with t parallel to \mathbf{B} except for $\theta_0 = 0$. In particular, the long-time average of $X_{C,3}(t)$ satisfies $\lim_{\tau \rightarrow \infty} (1/\tau) \int_0^\tau dt X_{C,3}(t) \geq 0$, which manifests chiral transport due to the CME. When \mathbf{S} is antiparallel to \mathbf{B} , i.e. $\theta_0 = \pi$, the wave packet occupies only the chiral band Ψ_0 and hence the linear dispersion gives a unidirectional motion $X_{C,3} \propto t$ (red curve in Fig. 4). When \mathbf{S} is parallel to \mathbf{B} , i.e., $\theta_0 = 0$, the initial state is a superposition of the particle and hole states $\Psi_{\pm 1}$. Therefore, the time evolution \bar{U}_F induces an oscillation with the frequency given by their energy difference 2ω , leading to a *Zitterbewegung* $X_{C,3} \propto \sin(2\omega t)$ of a Weyl fermion in a magnetic field (blue curve in Fig. 4) [59–62].

Experimental implementation.— With high scalability and controllability [63], ultracold atomic gases are excellent candidates for implementing the Floquet CME. The crucial ingredients are the spin-selective Thouless

pumps \mathcal{U}_j^\pm and $\mathcal{U}_{h,3}^\pm$, which can be realized by a spin-dependent optical lattice [64–68] or by laser-assisted tunneling [41, 69]. The unitary operator \mathcal{U}_q can be implemented by a sudden switch-on and -off of a quadrupole potential [56]. Let us discuss how to implement the spin-selective Thouless pumps $\mathcal{U}_j^\pm, \mathcal{U}_{h,3}^\pm$ by using a spin-dependent optical lattice. We consider atoms with two ground states trapped in a three-dimensional cubic optical lattice. To prevent the unwanted tunneling between lattice sites, we apply an optical field gradient [70] in three directions. The optical lattice is formed by a standing wave configuration produced by counterpropagating linearly polarized laser beams. Let θ_1 be the angle between the polarization vectors of the incoming and retroreflected laser beams in the x_1 direction and ϕ_1 be the locked phase of the incoming wave. By an adiabatic change of θ_1 (ϕ_1), the potential minima for atoms with $\sigma_1 = \pm 1$ move adiabatically in the opposite (same) directions [64–66], leading to spin (mass) transport. Therefore, U_1^\pm can be implemented by suitable changes of θ_1 and ϕ_1 . Similarly, the other pumps U_2^\pm and $U_{h,3}^\pm$ can be realized by changing the locked phases and the relative polarization angles. A detailed setup based on ^{87}Rb and yet another implementation using ^{173}Yb and helical pumps [41, 69, 71, 72] are discussed in Supplemental Material [73],

Classification of gapless Floquet states.— The emergence of a single Weyl fermion is a consequence of the nontrivial topology of the Floquet unitary. This phenomenon is generalized to a wider range of lattice-prohibited band structures under symmetries. In general, topologically nontrivial Floquet-Bloch operators as unitary maps from the Brillouin zone possess gapless quasienergy spectra, since a gapped Floquet operator can continuously be deformed into a trivial unitary, e.g. $U(\mathbf{k}) = 1_{N \times N}$ [30, 74]. Let us take a Floquet-Bloch operator $U(\mathbf{k}) := \mathcal{T} \exp[-i \int_0^T dt H(\mathbf{k}, t)] \in U(N)$ given by some unitary matrix. We consider three symmetries in the Altland-Zirnbauer classes [75, 76]: time-reversal symmetry $\Theta H(\mathbf{k}, t) \Theta^{-1} = H(-\mathbf{k}, T - t)$, particle-hole symmetry $CH(\mathbf{k}, t)C^{-1} = -H(-\mathbf{k}, t)$, and chiral symmetry $\Gamma H(\mathbf{k}, t) \Gamma^{-1} = -H(\mathbf{k}, T - t)$. In terms of the Floquet operators, these symmetries are expressed as $\Theta U(\mathbf{k}) \Theta^{-1} = U^\dagger(-\mathbf{k})$, $CU(\mathbf{k})C^{-1} = U(-\mathbf{k})$, and $\Gamma U(\mathbf{k}) \Gamma^{-1} = U^\dagger(\mathbf{k})$ [30]. We allow any continuous deformation of Floquet-Bloch operators which respect the symmetry of the system, and classify their stable equivalence classes according to the K-theory [75, 77]. Note that we do *not* assume energy gaps of the quasienergy band. Then, the classification of the unitary matrices can be performed in a manner similar to the classification of “unitary loops” for Floquet TIs/TSCs [78, 79]. We here outline the general idea and give the full derivation in Supplemental Material [80]. We define a Hermitian matrix $H_U(\mathbf{k})$ by

$$H_U(\mathbf{k}) = \begin{pmatrix} 0 & U(\mathbf{k}) \\ U^\dagger(\mathbf{k}) & 0 \end{pmatrix}, \quad (7)$$

which satisfies $H_U(\mathbf{k})^2 = 1_{2N \times 2N}$ and thus has eigen-

TABLE I: Tenfold-way topological classification of Floquet-Bloch operators for spatial dimension $d = 0, 1, 2, 3$. The Floquet single Weyl fermion in Eq. (4) corresponds to class A in $d = 3$.

class	$d = 0$	$d = 1$	$d = 2$	$d = 3$
A	0	\mathbb{Z}	0	\mathbb{Z}
AIII	\mathbb{Z}	0	\mathbb{Z}	0
AI	0	0	0	$2\mathbb{Z}$
BDI	\mathbb{Z}	0	0	0
D	\mathbb{Z}_2	\mathbb{Z}	0	0
DIII	\mathbb{Z}_2	\mathbb{Z}_2	\mathbb{Z}	0
AII	0	\mathbb{Z}_2	\mathbb{Z}_2	\mathbb{Z}
CII	$2\mathbb{Z}$	0	\mathbb{Z}_2	\mathbb{Z}_2
C	0	$2\mathbb{Z}$	0	\mathbb{Z}_2
CI	0	0	$2\mathbb{Z}$	0

values ± 1 . Note that in the case of the classification of Floquet TIs/TSCs, the unitary matrix is taken as $U(\mathbf{k}, t) := \mathcal{T} \exp[-i \int_0^t dt' H(\mathbf{k}, t')]$ instead of $U(\mathbf{k})$ [78]. Regarding $H_U(\mathbf{k})$ as a “Hamiltonian” and identifying its symmetry class, we can show that the classification of $U(\mathbf{k})$ is equivalent to that of $H_U(\mathbf{k})$ given by some K-groups of static TIs/TSCs. Using the K-group isomorphism between different spatial dimensions [75, 77], we find that the K-group of Floquet-Bloch operators of a symmetry class in d dimensions is given by that of static TIs/TSCs of the same symmetry class in $(d + 1)$ dimensions. Since the latter is equivalent to the classification of d -dimensional gapless surface states through the bulk-boundary correspondence, we arrive at the conclusion that the classification of d -dimensional gapless Floquet states is equivalent to that of d -dimensional gapless surface states of TIs/TSCs. The final result is summarized in Table I. This result strongly suggests that the gapless surface states of TIs/TSCs, which cannot have pure lattice realization without bulk, can be realized in bulk quasienergy spectra of periodically driven lattice systems. In fact, the single Weyl fermion presented in this paper corresponds to a surface state of a four-dimensional topological insulator [81]. It merits further study to explicitly construct examples of Floquet-Bloch operators and driving protocols in other symmetry classes.

Summary.— We have presented a periodically driven 3D lattice system that exhibits a single Weyl fermion in a quasienergy spectrum, thereby demonstrating a Floquet version of the CME. Our proposal utilizes the topology of the Floquet unitary. While the mathematical formula of the 3D winding number (5) was presented in a seminal work [30], its physical consequence and concrete realization had remained elusive. We have resolved this problem and provided a generalization to a topological classification of Floquet-Bloch operators in the Altland-Zirnbauer symmetry classes. We expect that the unique topological structure arising from unitary operators will serve as

a useful guideline for designing non-equilibrium systems free from the limitations of static phases of matter.

Acknowledgments

We thank I. Danshita, T. Tomita, Y. Ashida, Z. Gong, Y. Kikuchi, and T. Morimoto for fruitful discussions. We are especially grateful to K. Shiozaki for suggesting the generalization of our result by including symmetries. This work was supported by KAKENHI Grant No. JP18H01145 and a Grant-in-Aid for Scientific Research on Innovative Areas “Topological Materials Science (KAKENHI Grant No. JP15H05855) from the Japan Society for the Promotion of Science. S. H. acknowledges support from JSPS (Grant No. JP16J03619) and through the Advanced Leading Graduate Course for Photon Science (ALPS). M.N. is supported by RIKEN Special Postdoctoral Researcher Program.

Appendix A: Nontriviality of $U(\mathbf{k})$ as a map from \mathbb{T}^3 to $SU(2)$

It follows from the isomorphism $SU(2) \cong S^3$ that the element U in $SU(2)$ can be parametrized in terms of $\mathbf{u} = (u_1, u_2, u_3, u_4) \in S^3$ as

$$U = u_4 \sigma_0 + i(u_1 \sigma_1 + u_2 \sigma_2 + u_3 \sigma_3),$$

$$\sum_{k=1}^4 (u_k)^2 = 1. \quad (\text{A1})$$

If we parametrize $U(\mathbf{k})$ as

$$U(\mathbf{k}) = u_4(\mathbf{k}) \sigma_0 + i(u_1(\mathbf{k}) \sigma_1 + u_2(\mathbf{k}) \sigma_2 + u_3(\mathbf{k}) \sigma_3), \quad (\text{A2})$$

the winding number W defined in Eq. (5) in the main text can be expressed as

$$W = \int \frac{d\mathbf{k}}{2\pi^2} \sum_{i,j,k,l=1}^4 \epsilon_{ijkl} u_i(\mathbf{k}) \frac{\partial u_j(\mathbf{k})}{\partial k_1} \frac{\partial u_k(\mathbf{k})}{\partial k_2} \frac{\partial u_l(\mathbf{k})}{\partial k_3}, \quad (\text{A3})$$

where ϵ_{ijkl} is the totally antisymmetric tensor of rank 4 [42]. Expanding Eq. (4) in the main text, we obtain

$$\begin{aligned} u_1(\mathbf{k}) &= -\sin(k_1) \cos^2\left(\frac{k_2}{2}\right) \cos^2\left(\frac{k_3}{2}\right), \\ u_2(\mathbf{k}) &= -\cos^2\left(\frac{k_1}{2}\right) \sin(k_2) \cos\left(\frac{k_3}{2}\right) \\ &\quad + \frac{1}{2} \sin(k_1) \cos^2\left(\frac{k_2}{2}\right) \sin(k_3), \\ u_3(\mathbf{k}) &= -\frac{1}{2} \sin(k_1) \sin(k_2) \cos\left(\frac{k_3}{2}\right) \\ &\quad - \cos^2\left(\frac{k_1}{2}\right) \cos^2\left(\frac{k_2}{2}\right) \sin(k_3), \\ u_4(\mathbf{k}) &= 2 \cos^2\left(\frac{k_1}{2}\right) \cos^2\left(\frac{k_2}{2}\right) \cos^2\left(\frac{k_3}{2}\right) - 1. \end{aligned} \quad (\text{A4})$$

Substituting these into Eq. (A3), we obtain $W = 1$.

In general, a nontrivial map from \mathbb{T}^3 to S^3 can be constructed from the *smash product* [82]. It is a mathematical tool for constructing a manifold from two manifolds. Let X (Y) be a manifold and x_0 (y_0) be a point on X (Y). The smash product $X \wedge Y$ is defined as the product space $X \times Y$ with the space $(\{x_0\} \times Y) \cup (X \times \{y_0\})$ identified with a point on $X \times Y$. For example, the smash product $S^1 \wedge S^1$, with S^1 being a circle, is isomorphic to the two-dimensional sphere S^2 . We parametrize these two circles as

$$S^1 = \{k | -\pi \leq k \leq \pi\}, \quad S^1 = \{k' | -\pi \leq k' \leq \pi\}, \quad (\text{A5})$$

and take x_0 and y_0 as $k = \pm\pi$ and $k' = \pm\pi$, respectively. Then, the product space $S^1 \times S^1$ and its subspace,

$$\begin{aligned} (\{x_0\} \times Y) \cup (X \times \{y_0\}) &= \\ \{(\pm\pi, k') | -\pi \leq k' \leq \pi\} \cup \{(k, \pm\pi) | -\pi \leq k \leq \pi\}, \end{aligned} \quad (\text{A6})$$

are identified with the Brillouin zone \mathbb{T}^2 of a square lattice and its boundary, respectively. As we can obtain S^2 from \mathbb{T}^2 by wrapping up the square $[-\pi, \pi]^2$, the smash product $S^1 \wedge S^1$, i.e. the square $[-\pi, \pi]^2$ with its boundary identified with a point, is isomorphic to S^2 . The isomorphic mapping $f_{1,1}$ is given by

$$\begin{aligned} f_{1,1}(k, k') &:= \left[-2 \cos^2\left(\frac{k}{2}\right) \cos^2\left(\frac{k'}{2}\right) + 1 \right] \mathbf{n}_1 \\ &\quad - \cos^2\left(\frac{k}{2}\right) \sin(k') \mathbf{n}_2 - \sin(k) \cos\left(\frac{k'}{2}\right) \mathbf{n}_3, \end{aligned} \quad (\text{A7})$$

where $\mathbf{n}_1 = (1, 0, 0)^T$, $\mathbf{n}_2 = (0, 1, 0)^T$, and $\mathbf{n}_3 = (0, 0, 1)^T$ (the superscript T denotes the transpose) are the unit vectors in three orthogonal directions.

As shown below, the nontrivial map $U(\mathbf{k})$ is constructed from the following isomorphism [82]:

$$S^1 \wedge S^1 \wedge S^1 \cong S^2 \wedge S^1 \cong S^3. \quad (\text{A8})$$

Let $\boldsymbol{\xi} = (\xi_1, \xi_2, \xi_3)^T$ be a unit vector on S^2 , i.e., $\sum_{i=1}^3 (\xi_i)^2 = 1$, and $k_1 \in [-\pi, \pi] \cong S^1$. The isomorphic mapping $f: S^2 \times S^1 \rightarrow S^3$ of the second isomorphism in Eq. (A8) is given by

$$\begin{aligned} & f_{2,1}(\boldsymbol{\xi}, k_1) \\ &= \frac{\xi_1 - 1}{2} \sin(k_1) \mathbf{a}_1 + \cos\left(\frac{k_1}{2}\right) (\xi_3 \mathbf{a}_2 + \xi_2 \mathbf{a}_3) \\ & \quad - \left[\sin^2\left(\frac{k_1}{2}\right) + \cos^2\left(\frac{k_1}{2}\right) \xi_1 \right] \mathbf{a}_4, \end{aligned} \quad (\text{A9})$$

where $\mathbf{a}_i (i = 1, 2, 3, 4)$ are unit vectors in four dimensions defined by

$$\begin{aligned} \mathbf{a}_1 &= (1, 0, 0, 0)^T, & \mathbf{a}_2 &= (0, 1, 0, 0)^T, \\ \mathbf{a}_3 &= (0, 0, 1, 0)^T, & \mathbf{a}_4 &= (0, 0, 0, 1)^T. \end{aligned} \quad (\text{A10})$$

Then, the composition of $f_{1,1}$ and $f_{2,1}$ defined by

$$\tilde{\mathbf{u}}(\mathbf{k}) = f_{2,1} [f_{1,1}(k_2, k_3), k_1] \quad (\text{A11})$$

gives an isomorphic mapping between $S^1 \wedge S^1 \wedge S^1$ and S^3 . Since the isomorphic mapping $f_{2,1} [f_{1,1}(k_2, k_3), k_1]$ to S^3 naturally has a unit winding number and the domain of $S^1 \wedge S^1 \wedge S^1$ and that of \mathbb{T}^3 are both cuboid $[-\pi, \pi]^3$, $\tilde{\mathbf{u}}(\mathbf{k})$ has a unit winding number:

$$\begin{aligned} W &= \int \frac{d\mathbf{k}}{2\pi^2} \sum_{i,j,k,l=1}^4 \epsilon_{ijkl} \tilde{u}_i(\mathbf{k}) \frac{\partial \tilde{u}_j(\mathbf{k})}{\partial k_1} \frac{\partial \tilde{u}_k(\mathbf{k})}{\partial k_2} \frac{\partial \tilde{u}_l(\mathbf{k})}{\partial k_3} \\ &= 1. \end{aligned} \quad (\text{A12})$$

We note that $\tilde{\mathbf{u}}(\mathbf{k})$ stays constant on the boundary of the Brillouin zone $\mathbb{T}^3 = [-\pi, \pi]^3$:

$$\tilde{\mathbf{u}}(\mathbf{k}) = (0, 0, 0, -1). \quad (\text{A13})$$

We define a continuous deformation $\tilde{\mathbf{u}}_s(\mathbf{k}) := R_{23}(s k_1/2) \tilde{\mathbf{u}}(\mathbf{k})$ with a deformation parameter $s \in [0, 1]$, where $R_{23}(\theta)$ is a rotation matrix defined by

$$R_{23}(\theta) := \begin{pmatrix} 1 & 0 & 0 & 0 \\ 0 & \cos \theta & -\sin \theta & 0 \\ 0 & \sin \theta & \cos \theta & 0 \\ 0 & 0 & 0 & 1 \end{pmatrix}. \quad (\text{A14})$$

It follows from Eq. (A13) that $\tilde{\mathbf{u}}_s(\mathbf{k}) = (0, 0, 0, -1)$ on the boundary of \mathbb{T}^3 and hence $\tilde{\mathbf{u}}_s(\mathbf{k})$ is continuous on \mathbb{T}^3 . Also, combining Eqs. (A4), (A7), and (A9), we obtain

$$\begin{aligned} \tilde{\mathbf{u}}_{s=0}(\mathbf{k}) &= \tilde{\mathbf{u}}(\mathbf{k}), \\ \tilde{\mathbf{u}}_{s=1}(\mathbf{k}) &= \mathbf{u}(\mathbf{k}), \end{aligned} \quad (\text{A15})$$

where $\mathbf{u}(\mathbf{k})$ is defined in Eq. (A4). Therefore, $\mathbf{u}(\mathbf{k})$ is also an isomorphic mapping between $S^1 \wedge S^1 \wedge S^1$ and S^3 and has a unit winding number $W = 1$.

Appendix B: Boundary condition of the Floquet-Bloch operator $U(\mathbf{k})$

From

$$U_j^\pm(k) = e^{\frac{\mp ik}{2}} \left[P_j^\pm e^{\frac{\mp ik}{2}} + P_j^\mp e^{\frac{\pm ik}{2}} \right] = e^{\frac{\mp ik}{2}} V_j(k), \quad (\text{B1})$$

where $V_j(k) := e^{-i\frac{\sigma_j}{2}k}$, we have

$$\begin{aligned} U(\mathbf{k}) &= V_1(k_1) V_3\left(\frac{k_3}{2}\right) V_2(k_2) V_3\left(\frac{k_3}{2}\right) \\ & \quad \times V_1(k_1) V_3\left(\frac{k_3}{2}\right) V_2(k_2) V_3\left(\frac{k_3}{2}\right). \end{aligned} \quad (\text{B2})$$

Using $V_j(\pm\pi) = \mp i\sigma_j, \sigma_1 V_2(k)\sigma_1 = V_2(-k), \sigma_1 V_3(k)\sigma_1 = V_3(-k)$, we have

$$\begin{aligned} U(\pm\pi, k_2, k_3) &= -\sigma_1 V_3\left(\frac{k_3}{2}\right) V_2(k_2) V_3\left(\frac{k_3}{2}\right) \sigma_1 \\ & \quad \times V_3\left(\frac{k_3}{2}\right) V_2(k_2) V_3\left(\frac{k_3}{2}\right) \\ &= -V_3\left(-\frac{k_3}{2}\right) V_2(-k_2) V_3\left(-\frac{k_3}{2}\right) \\ & \quad \times V_3\left(\frac{k_3}{2}\right) V_2(k_2) V_3\left(\frac{k_3}{2}\right) = -\sigma_0. \end{aligned} \quad (\text{B3})$$

Similarly, we have

$$\begin{aligned} U(k_1, \pm\pi, k_3) &= -V_1(k_1) V_3\left(\frac{k_3}{2}\right) \sigma_2 V_3\left(\frac{k_3}{2}\right) V_1(k_1) \\ & \quad \times V_3\left(\frac{k_3}{2}\right) \sigma_2 V_3\left(\frac{k_3}{2}\right) \\ &= -V_1(k_1) V_3\left(\frac{k_3}{2}\right) V_3\left(\frac{-k_3}{2}\right) V_1(-k_1) \\ & \quad \times V_3\left(\frac{-k_3}{2}\right) V_3\left(\frac{k_3}{2}\right) = -\sigma_0, \end{aligned} \quad (\text{B4})$$

where we use $\sigma_2 V_1(k)\sigma_2 = V_1(-k)$ and $\sigma_2 V_3(k)\sigma_2 = V_3(-k)$ in the second and the third lines, respectively. By a straightforward calculation of the product of 2×2 matrices, we have

$$V_3\left(\pm\frac{\pi}{2}\right) V_2(k_2) V_3\left(\pm\frac{\pi}{2}\right) = \mp i\sigma_3 V_1(\pm k_2), \quad (\text{B5})$$

and thus we obtain

$$\begin{aligned} U(k_1, k_2, \pm\pi) &= V_1(k_1) [\mp i\sigma_3 V_1(\pm k_2)] V_1(k_1) [\mp i\sigma_3 V_1(\pm k_2)], \\ &= -V_1(k_1) V_1(\mp k_2) V_1(-k_1) V_1(\pm k_2) = -\sigma_0, \end{aligned} \quad (\text{B6})$$

which completes the derivation of the boundary condition $U(\mathbf{k}) = -\sigma_0$.

Appendix C: Wave-packet dynamics of a Weyl fermion without and with a magnetic field

1. Without a magnetic field

In the main text, the Floquet dynamics under \mathcal{U}_F is calculated from the initial state

$$\psi(\mathbf{k}, 0) = \left(\frac{1}{\pi(\delta k)^2} \right)^{\frac{3}{4}} e^{-\frac{|\mathbf{k}|^2}{2(\delta k)^2}} \mathbf{v}, \quad (\text{C1})$$

where δk denotes the width of the wave packet in momentum space with $\delta k \ll 1$ and \mathbf{v} specifies the spin state as $\mathbf{S} = \langle \mathbf{v}, \boldsymbol{\sigma} \mathbf{v} \rangle$. The center of mass at time $t = nT$ is then given by

$$\begin{aligned} & \mathbf{X}_C(t) \\ &= \int d\mathbf{k} \psi^\dagger(\mathbf{k}, t) [i\nabla_{\mathbf{k}} \psi(\mathbf{k}, t)] \\ &= \int d\mathbf{k} |\psi(\mathbf{k}, 0)|^2 \langle \mathbf{v}, \{ [U(\mathbf{k})]^n \}^\dagger i\nabla_{\mathbf{k}} [U(\mathbf{k})]^n \mathbf{v} \rangle \\ &+ \int d\mathbf{k} \psi^*(\mathbf{k}, 0) i\nabla_{\mathbf{k}} \psi(\mathbf{k}, 0) \\ &= \int d\mathbf{k} |\psi(\mathbf{k}, 0)|^2 \langle \mathbf{v}, \{ [U(\mathbf{k})]^n \}^\dagger i\nabla_{\mathbf{k}} [U(\mathbf{k})]^n \mathbf{v} \rangle. \end{aligned} \quad (\text{C2})$$

From $\delta k \ll 1$, $|\psi(\mathbf{k}, 0)|^2$ is approximated by the delta function $\delta(\mathbf{k})$, and we obtain

$$\begin{aligned} \mathbf{X}_C(t) &= \int d\mathbf{k} \delta(\mathbf{k}) \langle \mathbf{v}, \{ [U(\mathbf{k})]^n \}^\dagger i\nabla_{\mathbf{k}} [U(\mathbf{k})]^n \mathbf{v} \rangle \\ &= t \langle \mathbf{v}, i\nabla_{\mathbf{k}} U(\mathbf{k} = 0) \mathbf{v} \rangle = t\mathbf{S}, \end{aligned} \quad (\text{C3})$$

where we use $U(\mathbf{k}) = \sigma_0 - i\boldsymbol{\sigma} \cdot \mathbf{k} + \mathcal{O}(|\mathbf{k}|^2)$ in the last line.

2. With a magnetic field

The Schrödinger equation of a Weyl fermion subject to a magnetic field along the x_3 axis in continuous space is given by

$$\begin{aligned} i\partial_t \psi(\mathbf{x}, t) &= H\psi(\mathbf{x}, t), \\ H &= v\boldsymbol{\sigma} \cdot (-i\nabla + \mathbf{A}), \end{aligned} \quad (\text{C4})$$

where \mathbf{A} is a gauge potential representing a magnetic field $\mathbf{B} = (0, 0, -B)$ and v is the velocity of the Weyl fermion. When we take the Landau gauge $\mathbf{A} = (0, -Bx_1, 0)$, the momenta k_2 and k_3 remain good quantum numbers. The energy eigenvalues ϵ_n and the eigenstates Ψ_n of the Weyl

Hamiltonian H are given by

$$\begin{aligned} \epsilon_n &= \sqrt{(vk_3)^2 + n\omega^2}, \\ \Psi_n(k_3) &= \frac{1}{\sqrt{2l_B(\epsilon_n + vk_3)}} \begin{pmatrix} (\epsilon_n + vk_3)h_n(\bar{x}_1) \\ -i\omega\sqrt{n}h_{n-1}(\bar{x}_1) \end{pmatrix}, \\ \epsilon_0 &= vk_3, \\ \Psi_0(k_3) &= \frac{1}{\sqrt{l_B}} \begin{pmatrix} h_0(\bar{x}_1) \\ 0 \end{pmatrix}, \\ \epsilon_{-n} &= -\sqrt{(vk_3)^2 + n\omega^2}, \\ \Psi_{-n}(k_3) &= \frac{1}{\sqrt{2l_B(\epsilon_n - vk_3)}} \begin{pmatrix} (\epsilon_n - vk_3)h_n(\bar{x}_1) \\ i\omega\sqrt{n}h_{n-1}(\bar{x}_1) \end{pmatrix}, \end{aligned} \quad (\text{C5})$$

where $\bar{x}_1 := [x_1 - k_2(l_B)^2]/l_B$ with $l_B = 1/\sqrt{B}$ being the magnetic length, $\omega = v\sqrt{2B}$ is one half of the Landau gap, and $h_n(x_1)$ is the normalized Hermite function defined by

$$h_n(x_1) := \frac{1}{\sqrt{n!2^n\sqrt{\pi}}} H_n(x_1) e^{-\frac{(x_1)^2}{2}}. \quad (\text{C6})$$

Here H_n is the Hermite polynomial of order n . We consider an initial state given by

$$\psi(\mathbf{x}, 0) = \left(\frac{1}{\pi(l_B)^2} \right)^{\frac{1}{4}} \left(\frac{1}{\pi(r_0)^2} \right)^{\frac{1}{2}} e^{-\frac{(x_1)^2}{2(l_B)^2} - \frac{(x_2)^2 + (x_3)^2}{2(r_0)^2}} \mathbf{v}, \quad (\text{C7})$$

where the widths l_B and r_0 are chosen such that $r_0 \gg l_B \gg 1$. The spin state \mathbf{v} is written as $\mathbf{v} = [e^{-i\phi_0} \sin(\theta_0/2), \cos(\theta_0/2)]$, and satisfies $\langle \mathbf{v}, \boldsymbol{\sigma} \mathbf{v} \rangle = \mathbf{S} = (\sin\theta_0 \cos\phi_0, \sin\theta_0 \sin\phi_0, -\cos\theta_0)$, where \mathbf{S} specifies the direction of the spin of the initial state. Here, θ_0 is the angle between \mathbf{B} and \mathbf{S} , and ϕ_0 is the azimuth angle. Then, the initial state (C7) is expanded in terms of $\Psi_n(k_3)$ as

$$\begin{aligned} \psi(\mathbf{x}, 0) &= \int dk_2 dk_3 e^{i(k_2 x_2 + k_3 x_3)} \Phi_{r_0}(k_2) \Phi_{r_0}(k_3) \bar{\psi}(t=0, k_3) \\ \bar{\psi}(t=0, k_3) &= \sin(\theta_0/2) e^{-i\phi_0} \Psi_0(k_3) \\ &+ \frac{iv \cos(\theta_0/2)}{\epsilon_1 l_B} \left(\frac{\Psi_1(k_3)}{\sqrt{\epsilon_1 + vk_3}} - \frac{\Psi_{-1}(k_3)}{\sqrt{\epsilon_1 - vk_3}} \right), \end{aligned} \quad (\text{C8})$$

where $\Phi_{r_0}(k)$ represents a localized wave packet with width $(r_0)^{-1}$ in momentum space

$$\Phi_{r_0}(k) = \left(\frac{(r_0)^2}{\pi} \right)^{\frac{1}{4}} e^{-\frac{(r_0 k)^2}{2}}. \quad (\text{C9})$$

The wave function at time t is given by

$$\begin{aligned} \bar{\psi}(t, k_3) &= \sin(\theta_0/2) e^{-i\phi_0 - i\epsilon_0 t} \Psi_0(k_3) \\ &+ \frac{iv \cos(\theta_0/2)}{\epsilon_1 l_B} \left(\frac{e^{-i\epsilon_1 t} \Psi_1(k_3)}{\sqrt{\epsilon_1 + vk_3}} - \frac{e^{i\epsilon_1 t} \Psi_{-1}(k_3)}{\sqrt{\epsilon_1 - vk_3}} \right). \end{aligned} \quad (\text{C10})$$

For a sufficiently large width $r_0 \gg l_B$, the time evolution of the center of mass $X_{C,3}(t)$ along the x_3 direction is given by

$$\begin{aligned}
X_{C,3}(t) &= \int dx_1 dk_2 dk_3 |\Phi_{r_0}(k_2)|^2 |\Phi_{r_0}(k_3)|^2 \bar{\psi}^*(t, k_3) i \frac{\partial \bar{\psi}(t, k_3)}{\partial k_3} \\
&= i \int dx_1 \bar{\psi}^*(t, k_3 = 0) \frac{\partial \bar{\psi}(t, k_3 = 0)}{\partial k_3} \\
&= \sin^2\left(\frac{\theta_0}{2}\right) vt \int dx_1 |\Psi_0|^2 + \frac{i}{\sqrt{2}} \cos^2\left(\frac{\theta_0}{2}\right) \\
&\quad \times \int dx_1 [\Psi_1^* e^{i\omega t} - \Psi_{-1}^* e^{-i\omega t}] \frac{\partial}{\partial k_3} [\Psi_1 e^{-i\omega t} - \Psi_{-1} e^{i\omega t}] \\
&= \sin^2\left(\frac{\theta_0}{2}\right) vt \\
&\quad - \frac{i}{\sqrt{2\omega}} \cos^2\left(\frac{\theta_0}{2}\right) \left[e^{2i\omega t} \int dx_1 \Psi_1^* \frac{\partial \Psi_{-1}}{\partial k_3} + \text{c.c.} \right] \\
&= \sin^2\left(\frac{\theta_0}{2}\right) vt - \frac{v}{2\omega} \cos^2\left(\frac{\theta_0}{2}\right) \sin(2\omega t). \tag{C11}
\end{aligned}$$

In the units $a = T = 1$, we have $v = a/T = 1$ and hence obtain Eq. (6) in the main text from Eq. (C11). One can see from the second last line of Eq. (C11) that the oscillation $\sin(2\omega t)$ results from the interference between the particle band Ψ_1 and the hole band Ψ_{-1} . This is the so-called *Zitterbewegung*, which was originally discussed for a Dirac particle in the absence of a magnetic field [59], and later generalized to a relativistic particle under a magnetic field [61, 62].

Appendix D: Explicit form of $\bar{U}(k_2, k_3)$

The partial Fourier transform of $\mathcal{U}_q^\dagger \mathcal{U}_2^\pm \mathcal{U}_q$ and \mathcal{U}_1^\pm in the x_2 - and x_3 -axes are given by

$$\begin{aligned}
\mathcal{U}_q^\dagger \mathcal{U}_2^\pm \mathcal{U}_q &= \sum_{k_2, k_3} \sum_{x_1} c_{x_1}^\dagger U_2^\pm(k_2 - 2\pi\phi x_1) c_{x_1}, \\
\mathcal{U}_1^\pm &= \sum_{k_2, k_3} \sum_{x_1} \left(c_{x_1 \pm 1}^\dagger P_1^\pm c_{x_1} + c_{x_1}^\dagger P_1^\mp c_{x_1} \right), \tag{D1}
\end{aligned}$$

where $c_{x_1} := c_{x_1, k_2, k_3}$. Then, defining $V^\pm(x_1)$ as $V^\pm(x_1) := U_{h,3}^-(k_3) U_2^\pm(k_2 - 2\pi\phi x_1) U_{h,3}^+(k_3)$, we obtain

$$\begin{aligned}
\mathcal{U}_{h,3}^- \mathcal{U}_q^\dagger \mathcal{U}_2^\pm \mathcal{U}_q \mathcal{U}_{h,3}^+ &= \sum_{k_2, k_3} \sum_{x_1} c_{x_1}^\dagger V^\pm(x_1) c_{x_1}, \\
\bar{U}_F &= \mathcal{U}_1^- \mathcal{U}_{h,3}^- \mathcal{U}_q^\dagger \mathcal{U}_2^- \mathcal{U}_q \mathcal{U}_{h,3}^+ \mathcal{U}_1^+ \mathcal{U}_{h,3}^- \mathcal{U}_q^\dagger \mathcal{U}_2^+ \mathcal{U}_q \mathcal{U}_{h,3}^+ \\
&= \sum_{k_2, k_3} \bar{U}(k_2, k_3), \\
\bar{U}(k_2, k_3) &= \sum_{x_1} \left(c_{x_1+1}^\dagger \bar{u}_1 c_{x_1} + c_{x_1}^\dagger \bar{u}_0 c_{x_1} + c_{x_1-1}^\dagger \bar{u}_{-1} c_{x_1} \right), \\
\bar{u}_1 &= P_1^+ V^-(x_1 + 1) P_1^+ V^+(x_1), \\
\bar{u}_0 &= P_1^- V^-(x_1 + 1) P_1^+ V^+(x_1) + P_1^+ V^-(x_1) P_1^- V^+(x_1), \\
\bar{u}_{-1} &= P_1^- V^-(x_1) P_1^- V^+(x_1). \tag{D2}
\end{aligned}$$

This is a Floquet analogue of the Aubry-Andrei-Harper model [83, 84] with two parameters k_2 and k_3 . When the periodic boundary condition is imposed in the x_1 direction, a change in the momentum $k_2 \rightarrow k_2 + \Delta k$ is compensated by a shift along the x_1 direction $x_1 \rightarrow x_1 + \Delta k / (2\pi\phi)$.

Appendix E: Details of the experimental implementation

In this appendix, we discuss possible experimental implementations of the Floquet CME either by using a spin-dependent optical lattice with ^{87}Rb or by using laser-assisted tunneling with ^{173}Yb .

1. Setup with ^{87}Rb

As discussed in the main text, the main ingredient of our driving protocol is spin-dependent transport using spin-dependent optical lattices, which have already been realized with ^{87}Rb [67, 68]. The two spin states $|\uparrow\rangle$ and $|\downarrow\rangle$ are chosen as $|\uparrow\rangle = |F=2, m_F=-2\rangle$ and $|\downarrow\rangle = |F=1, m_F=-1\rangle$. Consider a 3D optical lattice produced by three orthogonal laser beams and their retroreflected ones. To suppress the natural hopping J , we apply an optical field gradient with a slope Δ , which is sufficiently small compared with the lattice depth V_0 but larger than J [70, 85]. The three pairs of counterpropagating plane waves are all linearly polarized, and we write the angle between the polarization vectors $\mathbf{e}_{1,+}^p$ and $\mathbf{e}_{1,-}^p$ of the beams along the x_1 axis as θ_1 , that along the x_2 axis as θ_2 , and that along the x_3 axis as θ_3 . Those angles are dynamically controlled by electro-optical modulators by rotating the polarization vector of the retroreflected laser beams. Then, the wave vectors $\mathbf{k}_{i,\alpha}$ ($i=1, 2, 3$ and $\alpha=+, -$) and the polarization vectors $\mathbf{e}_{i,\alpha}^p$ ($i=1, 2, 3$ and $\alpha=+, -$) of the six laser beams are given by

$$\begin{aligned}
\mathbf{k}_{1,\pm} &= \pm k \mathbf{n}_1, \quad \mathbf{e}_{1,\pm}^p = R_1 \left(\frac{\pm\theta_1}{2} \right) \mathbf{n}_2, \\
\mathbf{k}_{2,\pm} &= \pm k \mathbf{n}_2, \quad \mathbf{e}_{2,\pm}^p = R_2 \left(\frac{\pm\theta_2}{2} \right) \mathbf{n}_3, \\
\mathbf{k}_{3,\pm} &= \pm k \mathbf{n}_3, \quad \mathbf{e}_{3,\pm}^p = R_3 \left(\frac{\pm\theta_3}{2} \right) \mathbf{n}_1, \tag{E1}
\end{aligned}$$

where \mathbf{n}_i ($i=1, 2, 3$) is the unit vectors in the x_i axis and $R_i(\theta)$ is the rotation matrix around the x_i axis through angle θ (see Fig. 5).

Then, the created optical potential $U(\mathbf{x})$ at the position \mathbf{x} is given by

$$\begin{aligned}
U(\mathbf{x}) &= u_s |[\mathbf{e}^p(\mathbf{x})]^* \cdot \mathbf{e}^p(\mathbf{x})| \sigma_0 + u_v \mathbf{B}_{\text{eff}} \cdot \boldsymbol{\sigma}, \\
\mathbf{B}_{\text{eff}} &= i [\mathbf{e}^p(\mathbf{x})]^* \times \mathbf{e}^p(\mathbf{x}), \\
\mathbf{e}^p(\mathbf{x}) &= \sum_{i=1,2,3} \sum_{\alpha=\pm} \mathbf{e}_{i,\alpha}^p \exp(i\mathbf{k}_{i,\alpha} \cdot \mathbf{x} + \phi_i), \tag{E2}
\end{aligned}$$

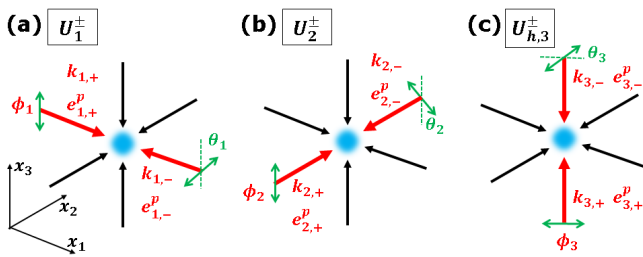


FIG. 5: Laser configurations of the spin-selective pumps (a) U_1^\pm , (b) U_2^\pm , and (c) $U_{h,3}^\pm$, where $\mathbf{k}_{i,\alpha}$ and $\mathbf{e}_{i,\alpha}^p$ ($i = 1, 2, 3$ and $\alpha = +, -$) are the wave vectors and the polarization vectors of the six linearly polarized laser beams forming an optical lattice. The red and black arrows represent the wave vectors of the counterpropagating laser beams and green arrows are their polarization directions, and θ_i denotes the angle between $\mathbf{e}_{i,+}^p$ and $\mathbf{e}_{i,-}^p$, and ϕ_i denotes the locked phase of the incoming wave along the x_i axis.

where u_s , u_v , σ_0 , and $\boldsymbol{\sigma}$ are the scalar potential, the vector potential, the 2×2 identity matrix, and the Pauli matrix vector with respect to the spin states $|\uparrow\rangle$ and $|\downarrow\rangle$, respectively [86]. Here, ϕ_i is the phase of the incoming wave along the x_i axis that is phase-locked and controlled by an additional electro-optical modulator. We first consider the spin transport along the x_1 -axis through the changes of θ_1 and ϕ_1 . Suppose $u_s > u_v > 0$ and we initially set $\theta_1 = \theta_2 = \theta_3 = 0$ and $\phi_1 = \phi_2 = \phi_3 = \pi$. In this case, the atoms are trapped at $\mathbf{x} = a(m_1, m_2, m_3) \in a\mathbb{Z}^3$, where $a = \pi/k$ is the lattice constant. As we change (θ_1, ϕ_1) from $(0, \pi)$ to $(\pi, 2\pi)$, atoms with spin states $\sigma_1 = 1$ are displaced by one lattice site in the positive x_1 direction, while those with spin states $\sigma_1 = -1$ are not, realizing spin-selective transport for spin states $\sigma_1 = 1$. For the parameter change of (θ_1, ϕ_1) from $(0, \pi)$ to $(\pi, 0)$, atoms with spin states $\sigma_1 = -1$ are displaced by one lattice site in the negative x_1 direction, while those with spin states $\sigma_1 = 1$ are not, realizing a spin-selective transport for spin states $\sigma_1 = -1$. The spin-selective transport along the x_2 - and x_3 -directions can be achieved by changing (θ_2, ϕ_2) and (θ_3, ϕ_3) , respectively.

To observe of the Floquet CME, the time scale of the pump τ_{pump} should be made much smaller than the decoherence time τ_{de} . The time scale of the pump τ_{pump} is determined from the adiabaticity condition of sliding of the lattice, i.e., avoiding the excitation to higher Bloch bands. This condition is satisfied for $\tau_{\text{pump}} \geq 40 \mu\text{sec}$ for the lattice depth $V_0 = 30E_r$, with E_r being the recoil energy [67, 68]. The dominant mechanism for decoherence may be the on-site interaction between particles [67], by which $\tau_{\text{de}} = 200 \mu\text{sec}$ for the lattice depth $V_0 = 25E_r$ with E_r being the recoil energy of ^{87}Rb with wavelength $\lambda = 785 \text{ nm}$. When the single spin-selective Thouless pump operates within $40 \mu\text{sec}$, atoms experience the interaction energy during the time $\tau_{d,s} = 40 \mu\text{sec} \times (w/\lambda)$ with w being the size of a wave packet localized at a site. Then, the total time $\tau_{d,\text{tot}}$ during which the atoms ex-

perience the interaction is estimated to be $\tau_{d,\text{tot}} = 8\tau_{d,s}$. Since $(w/\lambda) \approx \sqrt{V_0/E_r}$ for a deep optical lattice and the interaction energy $\propto \tau_{\text{de}}^{-1}$ is proportional to $(V_0/E_r)^{\frac{4}{3}}$ [63], $\tau_{\text{de}}/\tau_{d,\text{tot}} = 8$ for the lattice depth $V_0/E_r = 20$. In this case, the optical field gradient with the on-site energy difference Δ with tens of kHz is sufficient to suppress the natural hopping $J = 0.02E_r \sim \text{kHz}$. Thus, 8 cycles of the pumps can operate, which is sufficient to observe the displacement of the center of mass shown in Fig. 4. Another limitation is the excitation to higher Bloch bands due to the quadrupole field pulse. The weight w_{exc} of the excited states is $w_{\text{exc}} \propto \phi(w/\lambda)^2$ [56] and hence it is negligible for a weak magnetic flux and a deep optical lattice.

2. Setup with ^{173}Yb

Motivated by the recent experiments on realizing synthetic gauge fields [87, 88] and the proposals for implementing a helical hopping [41, 69], we consider yet another implementation scheme using fermionic alkaline-earth-like atoms ^{173}Yb and a laser-assisted hopping using the excited level 3P_1 . The two spin states are taken as $|m_F = -5/2\rangle$ and $|m_F = -1/2\rangle$ in the ground state manifold 1S_0 with $F = I = 5/2$. The six-fold degeneracy between the spin states is lifted by a Zeeman splitting $\Delta_{B,3}$ induced by a uniform magnetic field in the x_3 direction. The natural hopping is suppressed by a magnetic field gradient $\delta B_3 = \Delta_1 x_1 + \Delta_2 x_2 + \Delta_3 x_3$, where Δ_1, Δ_2 , and Δ_3 are the on-site energy difference along the x_1 , x_2 , and x_3 directions, respectively. For a lattice depth $V_0 = 20E_r$, where the natural hopping J is given by $J = 0.02E_r$, the Zeeman splitting $\Delta_{B,z}$ of the order of tens of kHz is sufficient for the suppression. A spin-flip hopping along the x_3 direction can be induced by Raman laser beams resonant to the energy difference Δ_3 [69]. The helical pump can be implemented by this spin-flip hopping followed by the π pulse [41]. The helical hoppings in the other two directions can be implemented by a combination of the $\pi/2$ pulses and the helical pump. One can selectively induce these three directional hoppings by making Δ_1, Δ_2 , and Δ_3 different from each other and three pairs of Raman laser beams. This can be done also by a pair of Raman laser beams and dynamically changing Δ_1, Δ_2 , and Δ_3 .

To observe the Floquet CME, the time scale of the pump τ_{pump} should be made much smaller than the lifetime τ_{life} of the Raman induced hopping. The time scale of a Raman-induced hopping Ω on a lattice system is of the order of kHz [87] when the one-photon detuning δ of the Raman process is taken to be of the order of 1 GHz [69, 88]. In this case, the single pump operates within one msec, leading to tens of msec for one cycle of the pump. The lifetime $\tau_{\text{life}} \sim \delta/(\gamma\Omega)$ due to heating with the Raman process is of the order of 1 sec for the lifetime of $\gamma = 850 \text{ nsec}$ [89], which is much longer than the alkali-metal system [88]. Therefore, at least a few tens of

pumps can operate within the lifetime. This is sufficient for the observation of the Floquet CME.

Appendix F: K-group correspondence in the classification of gapless Floquet states

In this appendix, we derive the K-group correspondence between gapless Floquet states and static TIs/TSCs. The derivation proceeds in a manner similar to that for Floquet TIs/TSCs given in Refs. 78 and 79. As mentioned in the main text, we construct a Hermitian matrix

$$H_U(\mathbf{k}) = \begin{pmatrix} 0 & U(\mathbf{k}) \\ U^\dagger(\mathbf{k}) & 0 \end{pmatrix} \quad (\text{F1})$$

from the Floquet-Bloch operator $U(\mathbf{k})$. This Hamiltonian has the following chiral symmetry:

$$\Gamma_2 H_U(\mathbf{k}) \Gamma_2^{-1} = -H_U(\mathbf{k}), \quad (\text{F2})$$

where

$$\Gamma_2 = \begin{pmatrix} 1_{N \times N} & 0 \\ 0 & -1_{N \times N} \end{pmatrix}. \quad (\text{F3})$$

Therefore, the classification of class A (i.e. no symmetry) Floquet-Bloch operators in d dimensions is equivalent to that of class AIII topological insulators in d dimensions. When the Floquet operator has the time-reversal symmetry (TRS) $\Theta U(\mathbf{k}) \Theta^{-1} = U^\dagger(-\mathbf{k})$ with $\epsilon_\Theta := \Theta^2 = \pm 1$, the Hamiltonian $H_U(\mathbf{k})$ has the following symmetries

$$\Theta_1 H_U(\mathbf{k}) \Theta_1^{-1} = H_U(-\mathbf{k}), \quad (\text{F4})$$

$$\Theta_2 H_U(\mathbf{k}) \Theta_2^{-1} = -H_U(-\mathbf{k}), \quad (\text{F5})$$

where

$$\Theta_1 := \begin{pmatrix} 0 & \Theta \\ \Theta & 0 \end{pmatrix}, \quad \Theta_2 := \begin{pmatrix} 0 & \Theta \\ -\Theta & 0 \end{pmatrix}. \quad (\text{F6})$$

These symmetries are regarded as effective time-reversal symmetry and particle-hole symmetry of $H_U(\mathbf{k})$. Since $\Theta_1^2 = \epsilon_\Theta$ and $\Theta_2^2 = -\epsilon_\Theta$, the classification of class AI (AII) Floquet-Bloch operators in d dimensions corresponds to that of class CI (DIII) topological superconductors in the same dimensions. Similarly, when $U(\mathbf{k})$ has the particle-hole symmetry (PHS) $C U(\mathbf{k}) C^{-1} = U(-\mathbf{k})$ with $\epsilon_C := C^2 = \pm 1$, we can define

$$C_1 := \begin{pmatrix} C & 0 \\ 0 & C \end{pmatrix}, \quad C_2 := \epsilon_C C_1 \Gamma_2 = \epsilon_C \begin{pmatrix} C & 0 \\ 0 & -C \end{pmatrix}, \quad (\text{F7})$$

so that

$$C_1 H_U(\mathbf{k}) C_1^{-1} = H_U(-\mathbf{k}), \quad (\text{F8})$$

$$C_2 H_U(\mathbf{k}) C_2^{-1} = -H_U(-\mathbf{k}), \quad (\text{F9})$$

with $C_1^2 = C_2^2 = \epsilon_C$. Therefore, the classification of class D (C) Floquet-Bloch operators in d dimensions corresponds to that of class BDI (CII) topological superconductors in the same dimensions.

Next, we consider the cases where the Floquet-Bloch operator has the chiral symmetry $\Gamma U(\mathbf{k}) \Gamma^{-1} = U^\dagger(\mathbf{k})$. Then, the Hamiltonian $H_U(\mathbf{k})$ satisfies

$$\Gamma_1 H_U(\mathbf{k}) \Gamma_1^{-1} = -H_U(\mathbf{k}) \quad (\text{F10})$$

with

$$\Gamma_1 := \begin{pmatrix} 0 & \Gamma \\ -\Gamma & 0 \end{pmatrix}, \quad (\text{F11})$$

which is another chiral symmetry of the Hamiltonian. By combining the two chiral symmetries (F2) and (F10), we have

$$\Gamma_1 \Gamma_2 H_U(\mathbf{k}) (\Gamma_1 \Gamma_2)^{-1} = H_U(\mathbf{k}) \quad (\text{F12})$$

and therefore the Hamiltonian $H_U(\mathbf{k})$ can be diagonalized simultaneously with $\Gamma_1 \Gamma_2$ such that

$$\tilde{\Gamma} := \Gamma_1 \Gamma_2 = \gamma \begin{pmatrix} 1_{N \times N} & 0 \\ 0 & -1_{N \times N} \end{pmatrix}. \quad (\text{F13})$$

Here, since $\tilde{\Gamma}^2 = -\Gamma_1^2 \Gamma_2^2 = \Gamma^2$, the eigenvalues $\pm \gamma$ are $\gamma = 1$ for $\Gamma^2 = 1$ and $\gamma = i$ for $\Gamma^2 = -1$. Since $\{\Gamma_1, \Gamma_2\} = 0$ and therefore $\{\tilde{\Gamma}, \Gamma_1\} = \{\tilde{\Gamma}, \Gamma_2\} = 0$, we can choose the basis such that

$$\Gamma_1 = i\gamma \begin{pmatrix} 0 & 1_{N \times N} \\ 1_{N \times N} & 0 \end{pmatrix}, \quad \Gamma_2 = \begin{pmatrix} 0 & -i1_{N \times N} \\ i1_{N \times N} & 0 \end{pmatrix} \quad (\text{F14})$$

(note that $\Gamma_1^2 = -\gamma^2$). In this basis, the Hamiltonian should have the form

$$H_U(\mathbf{k}) = \begin{pmatrix} A(\mathbf{k}) & 0 \\ 0 & -A(\mathbf{k}) \end{pmatrix} \quad (\text{F15})$$

to satisfy the chiral symmetries (F2) and (F10). Thus, the classification of $H_U(\mathbf{k})$ reduces to that of $A(\mathbf{k})$. For example, if the Floquet-Bloch operator has the chiral symmetry only (i.e. class AIII), $A(\mathbf{k})$ is a Hamiltonian without symmetry. Therefore, the classification of class AIII Floquet-Bloch operators in d dimensions reduces to that of class A topological insulators in the same dimensions. For the remaining classes, where the Floquet-Bloch operators have TRS, PHS, and the chiral symmetry, we identify the symmetry of $A(\mathbf{k})$ by using $\Gamma^2 = (\Theta C)^2 = \epsilon_\Theta \epsilon_C$ (here we assume that $[\Theta, C] = 0$). When $\epsilon_\Theta \epsilon_C = 1$ (i.e. $\gamma = 1$), Θ_1 and C_1 are symmetries of $A(\mathbf{k})$ since Θ_2 and C_2 flip the eigenvalue of $\tilde{\Gamma}$ due to $\{C_2, \tilde{\Gamma}\} = \{\Theta_2, \tilde{\Gamma}\} = 0$. Since $\Theta_1 C_1 = -\Gamma_1 \Gamma_2 = -\tilde{\Gamma}$ and $\tilde{\Gamma}$ has already been diagonalized, one of Θ_1 and C_1 is an independent symmetry. If we take C_1 , Eq. (F8) leads to

$$C A(\mathbf{k}) C^{-1} = A(-\mathbf{k}) \quad (\text{F16})$$

and this is the TRS of $A(\mathbf{k})$. Therefore, the classification of class BDI (CII) Floquet-Bloch operators in d dimensions is mapped to that of d -dimensional class AI (AII) topological insulators. On the other hand, when $\epsilon_{\Theta C} = -1$ (i.e. $\gamma = i$), the antiunitariness of TRS and PHS indicates that Θ_2 and C_2 preserve the eigenvalue of $\tilde{\Gamma}$, but that neither Θ_1 nor C_1 does it. Since $\Theta_2 C_2 = \Gamma_1 \Gamma_2 = \tilde{\Gamma}$, we consider only C_2 . Then, Eq. (F9) gives

$$CA(\mathbf{k})C^{-1} = -A(-\mathbf{k}), \quad (\text{F17})$$

which is the PHS of $A(\mathbf{k})$. Thus we find that the classification of class DIII (CI) Floquet-Bloch operators in d dimensions is equivalent to that of class D (C) topological superconductors in the same dimensions.

We thus obtain the following results on the classification of Floquet-Bloch operators. We denote the K-group of the Floquet-Bloch operators by $K_{\mathbb{F}}^{\text{FB}}(s, d)$, where d is the spatial dimension and (\mathbb{F}, s) represents the Altland-Zirnbauer symmetry class. To be concrete, $\mathbb{F} = \mathbb{C}$ with $s = 0, 1 \pmod{2}$ corresponds to the complex class (A, AIII), and $\mathbb{F} = \mathbb{R}$ with $s = 0, 1, \dots, 7 \pmod{8}$ corresponds to the real class (AI, BDI, D, DIII, AII, CII, C, CI). Similarly, we denote the K-group of static TIs/TSCs by $K_{\mathbb{F}}(s, d)$. Then, the analyses in this section indicate

that

$$K_{\mathbb{F}}^{\text{FB}}(s, d) = K_{\mathbb{F}}(s - 1, d). \quad (\text{F18})$$

We list the resulting classification of Floquet-Bloch operators in Table I in the main text. Using the K-group isomorphism $K_{\mathbb{F}}(s - 1, d) = K_{\mathbb{F}}(s, d + 1)$ [75, 77], we obtain

$$K_{\mathbb{F}}^{\text{FB}}(s, d) = K_{\mathbb{F}}(s, d + 1), \quad (\text{F19})$$

which shows the equivalence between the class of gapless bulk states in Floquet systems and that of surface gapless states of static TIs/TSCs.

Finally, we note that the classification of gapless Floquet states in d dimensions coincides with that of anomalous edge (or surface) states of Floquet TIs/TSCs given by unitary loops in $(d + 1)$ dimensions [78]. Indeed, it has been discussed that the gapless Floquet spectrum can be realized as the edge state of the anomalous Floquet TIs/TSCs [31]. We may interpret our result to be a generalization of this correspondence to all the Altland-Zirnbauer classes. The correspondence between the gapless topological singularities and topologically nontrivial unitaries has been discussed in the context of anomalous Floquet TIs/TSCs [74, 78].

-
- [1] H. Nielsen and M. Ninomiya, Nuclear Physics B **185**, 20 (1981), ISSN 0550-3213, URL <http://www.sciencedirect.com/science/article/pii/0550321381903618>.
- [2] H. Nielsen and M. Ninomiya, Nuclear Physics B **193**, 173 (1981), ISSN 0550-3213, URL <http://www.sciencedirect.com/science/article/pii/0550321381905241>.
- [3] S. Murakami, New Journal of Physics **9**, 356 (2007), URL <http://stacks.iop.org/1367-2630/9/i=9/a=356>.
- [4] X. Wan, A. M. Turner, A. Vishwanath, and S. Y. Savrasov, Phys. Rev. B **83**, 205101 (2011), URL <https://link.aps.org/doi/10.1103/PhysRevB.83.205101>.
- [5] H. Nielsen and M. Ninomiya, Physics Letters B **130**, 389 (1983), ISSN 0370-2693, URL <http://www.sciencedirect.com/science/article/pii/0370269383915290>.
- [6] A. A. Zyuzin and A. A. Burkov, Phys. Rev. B **86**, 115133 (2012), URL <https://link.aps.org/doi/10.1103/PhysRevB.86.115133>.
- [7] D. T. Son and N. Yamamoto, Phys. Rev. Lett. **109**, 181602 (2012), URL <https://link.aps.org/doi/10.1103/PhysRevLett.109.181602>.
- [8] A. A. Burkov, Phys. Rev. Lett. **113**, 247203 (2014), URL <https://link.aps.org/doi/10.1103/PhysRevLett.113.247203>.
- [9] B. Q. Lv, H. M. Weng, B. B. Fu, X. P. Wang, H. Miao, J. Ma, P. Richard, X. C. Huang, L. X. Zhao, G. F. Chen, et al., Phys. Rev. X **5**, 031013 (2015), URL <https://link.aps.org/doi/10.1103/PhysRevX.5.031013>.
- [10] S.-Y. Xu, I. Belopolski, N. Alidoust, M. Neupane, G. Bian, C. Zhang, R. Sankar, G. Chang, Z. Yuan, C.-C. Lee, et al., Science **349**, 613 (2015), ISSN 0036-8075, URL <http://science.sciencemag.org/content/349/6248/613>.
- [11] B. Q. Lv, N. Xu, H. M. Weng, J. Z. Ma, P. Richard, X. C. Huang, L. X. Zhao, G. F. Chen, C. E. Matt, F. Bisti, et al., Nat. Phys. **11**, 724 (2015), URL <https://www.nature.com/articles/nphys3426>.
- [12] L. X. Yang, Z. K. Liu, Y. Sun, H. Peng, H. F. Yang, T. Zhang, B. Zhou, Y. Zhang, Y. F. Guo, M. Rahn, et al., Nat. Phys. **11**, 728 (2015), URL <https://www.nature.com/articles/nphys3425>.
- [13] S.-Y. Xu, I. Belopolski, D. S. Sanchez, M. Neupane, G. Chang, K. Yaji, Z. Yuan, C. Zhang, K. Kuroda, G. Bian, et al., Phys. Rev. Lett. **116**, 096801 (2016), URL <https://link.aps.org/doi/10.1103/PhysRevLett.116.096801>.
- [14] N. Xu, H. M. Weng, B. Q. Lv, C. E. Matt, J. Park, F. Bisti, V. N. Strocov, D. Gawryluk, E. Pomjakushina, K. Conder, et al., Nat. Commun. **7**, 11006 (2016), URL <https://www.nature.com/articles/ncomms11006>.
- [15] S.-M. Huang, S.-Y. Xu, I. Belopolski, C.-C. Lee, G. Chang, B. Wang, N. Alidoust, G. Bian, M. Neupane, C. Zhang, et al., Nat. Commun. **6**, 7373 (2015), URL <https://www.nature.com/articles/ncomms8373>.
- [16] X. Huang, L. Zhao, Y. Long, P. Wang, D. Chen, Z. Yang, H. Liang, M. Xue, H. Weng, Z. Fang, et al., Phys. Rev. X **5**, 031023 (2015), URL <https://link.aps.org/doi/10.1103/PhysRevX.5.031023>.
- [17] F. Arnold, C. Shekhar, S.-C. Wu, Y. Sun, R. D. dos Reis, N. Kumar, M. Naumann, M. O. Ajeesh, M. Schmidt,

- A. G. Grushin, et al., Nat. Commun. **7**, 11615 (2016), URL <https://www.nature.com/articles/ncomms11615>.
- [18] Z. Wang, Y. Zheng, Z. Shen, Y. Lu, H. Fang, F. Sheng, Y. Zhou, X. Yang, Y. Li, C. Feng, et al., Phys. Rev. B **93**, 121112 (2016), URL <https://link.aps.org/doi/10.1103/PhysRevB.93.121112>.
- [19] C.-L. Zhang, S.-Y. Xu, I. Belopolski, Z. Yuan, Z. Lin, B. Tong, G. Bian, N. Alidoust, C.-C. Lee, S.-M. Huang, et al., Nature Communications **7**, 10735 (2016), URL <http://dx.doi.org/10.1038/ncomms10735><http://10.0.4.14/ncomms10735><https://www.nature.com/articles/ncomms10735>{\#supplementary-information}.
- [20] K. Fukushima, D. E. Kharzeev, and H. J. Warringa, Phys. Rev. D **78**, 074033 (2008), URL <https://link.aps.org/doi/10.1103/PhysRevD.78.074033>.
- [21] M. M. Vazifeh and M. Franz, Phys. Rev. Lett. **111**, 027201 (2013), URL <https://link.aps.org/doi/10.1103/PhysRevLett.111.027201>.
- [22] P. Goswami, G. Sharma, and S. Tewari, Phys. Rev. B **92**, 161110 (2015), URL <https://link.aps.org/doi/10.1103/PhysRevB.92.161110>.
- [23] K. Taguchi, T. Imaeda, M. Sato, and Y. Tanaka, Phys. Rev. B **93**, 201202 (2016), URL <https://link.aps.org/doi/10.1103/PhysRevB.93.201202>.
- [24] H. Sumiyoshi and S. Fujimoto, Phys. Rev. Lett. **116**, 166601 (2016), URL <https://link.aps.org/doi/10.1103/PhysRevLett.116.166601>.
- [25] Y. Ibe and H. Sumiyoshi, Journal of the Physical Society of Japan **86**, 054707 (2017), URL <https://doi.org/10.7566/JPSJ.86.054707>.
- [26] A. Cortijo, D. Kharzeev, K. Landsteiner, and M. A. H. Vozmediano, Phys. Rev. B **94**, 241405 (2016), URL <https://link.aps.org/doi/10.1103/PhysRevB.94.241405>.
- [27] D. I. Pikulin, A. Chen, and M. Franz, Phys. Rev. X **6**, 041021 (2016), URL <https://link.aps.org/doi/10.1103/PhysRevX.6.041021>.
- [28] T. Meng and J. C. Budich, arXiv preprint [arXiv:1804.05078](https://arxiv.org/abs/1804.05078) (2018).
- [29] A. Eckardt, Rev. Mod. Phys. **89**, 011004 (2017), URL <https://link.aps.org/doi/10.1103/RevModPhys.89.011004>.
- [30] T. Kitagawa, E. Berg, M. Rudner, and E. Demler, Phys. Rev. B **82**, 235114 (2010), URL <https://link.aps.org/doi/10.1103/PhysRevB.82.235114>.
- [31] M. S. Rudner, N. H. Lindner, E. Berg, and M. Levin, Phys. Rev. X **3**, 031005 (2013), URL <https://link.aps.org/doi/10.1103/PhysRevX.3.031005>.
- [32] D. V. Else, B. Bauer, and C. Nayak, Phys. Rev. Lett. **117**, 090402 (2016), URL <https://link.aps.org/doi/10.1103/PhysRevLett.117.090402>.
- [33] N. Y. Yao, A. C. Potter, I.-D. Potirniche, and A. Vishwanath, Phys. Rev. Lett. **118**, 030401 (2017), URL <https://link.aps.org/doi/10.1103/PhysRevLett.118.030401>.
- [34] D. J. Thouless, Phys. Rev. B **27**, 6083 (1983), URL <https://link.aps.org/doi/10.1103/PhysRevB.27.6083>.
- [35] S. Nakajima, T. Tomita, S. Taie, T. Ichinose, H. Ozawa, L. Wang, M. Troyer, and Y. Takahashi, Nat. Phys. **12**, 296 (2016), URL <http://www.nature.com/articles/nphys3622>.
- [36] M. Lohse, C. Schweizer, O. Zilberberg, M. Aidelsburger, and I. Bloch, Nat. Phys. **12**, 350 (2016), URL <http://www.nature.com/articles/nphys3584>.
- [37] X.-L. Qi and S.-C. Zhang, Rev. Mod. Phys. **83**, 1057 (2011), URL <https://link.aps.org/doi/10.1103/RevModPhys.83.1057>.
- [38] S. Ryu and S.-C. Zhang, Phys. Rev. B **85**, 245132 (2012), URL <https://link.aps.org/doi/10.1103/PhysRevB.85.245132>.
- [39] O. M. Sule, X. Chen, and S. Ryu, Phys. Rev. B **88**, 075125 (2013), URL <https://link.aps.org/doi/10.1103/PhysRevB.88.075125>.
- [40] C.-T. Hsieh, G. Y. Cho, and S. Ryu, Phys. Rev. B **93**, 075135 (2016), URL <https://link.aps.org/doi/10.1103/PhysRevB.93.075135>.
- [41] J. C. Budich, Y. Hu, and P. Zoller, Phys. Rev. Lett. **118**, 105302 (2017), URL <https://link.aps.org/doi/10.1103/PhysRevLett.118.105302>.
- [42] N. Manton and P. Sutcliffe, *Topological solitons* (Cambridge University Press, Cambridge, 2004).
- [43] See Supplemental Material, App. A for the derivation and the method of constructing a nontrivial map to S^3 .
- [44] See Supplemental Material, App. B for the detailed derivation.
- [45] C.-K. Chan, Y.-T. Oh, J. H. Han, and P. A. Lee, Phys. Rev. B **94**, 121106 (2016), URL <https://link.aps.org/doi/10.1103/PhysRevB.94.121106>.
- [46] H. Hübener, M. A. Sentef, U. De Giovannini, A. F. Kemper, and A. Rubio, Nature Communications **8**, 13940 (2017), URL <http://dx.doi.org/10.1038/ncomms13940><http://10.0.4.14/ncomms13940><https://www.nature.com/articles/ncomms13940>{\#supplementary-information}.
- [47] H. Wang, L. Zhou, and Y. D. Chong, Phys. Rev. B **93**, 144114 (2016), URL <https://link.aps.org/doi/10.1103/PhysRevB.93.144114>.
- [48] J.-Y. Zou and B.-G. Liu, Phys. Rev. B **93**, 205435 (2016), URL <https://link.aps.org/doi/10.1103/PhysRevB.93.205435>.
- [49] L. Bucciantini, S. Roy, S. Kitamura, and T. Oka, Phys. Rev. B **96**, 41126 (2017), URL <https://link.aps.org/doi/10.1103/PhysRevB.96.41126>.
- [50] R. Wang, B. Wang, R. Shen, L. Sheng, and D. Y. Xing, EPL (Europhysics Letters) **105**, 17004 (2014), URL <http://stacks.iop.org/0295-5075/105/i=1/a=17004>.
- [51] S. Ebihara, K. Fukushima, and T. Oka, Phys. Rev. B **93**, 155107 (2016), URL <https://link.aps.org/doi/10.1103/PhysRevB.93.155107>.
- [52] X.-X. Zhang, T. T. Ong, and N. Nagaosa, Phys. Rev. B **94**, 235137 (2016), URL <https://link.aps.org/doi/10.1103/PhysRevB.94.235137>.
- [53] Z. Yan and Z. Wang, Phys. Rev. Lett. **117**, 87402 (2016), URL <https://link.aps.org/doi/10.1103/PhysRevLett.117.087402>.
- [54] K. Takasan, M. Nakagawa, and N. Kawakami, Phys. Rev. B **96**, 115120 (2017), URL <https://link.aps.org/doi/10.1103/PhysRevB.96.115120>.
- [55] See Supplemental Material, App. C.1 for the detailed derivation.
- [56] A. S. Sorensen, E. Demler, and M. D. Lukin, Phys. Rev. Lett. **94**, 86803 (2005), URL <https://link.aps.org/doi/10.1103/PhysRevLett.94.086803>.
- [57] See Supplemental Material, App. D for the explicit form of $\bar{U}(k_2, k_3)$.
- [58] See Supplemental Material, App. C.2 for the detailed

derivation.

- [59] E. Schrödinger, Sitz. Preuss. Akad. Wiss. Phys.Math. Kl. **24**, 418 (1930).
- [60] R. Gerritsma, G. Kirchmair, F. Zähringer, E. Solano, R. Blatt, and C. F. Roos, Nature **463**, 68 (2010), URL <http://dx.doi.org/10.1038/nature08688><http://10.0.4.14/nature08688>.
- [61] A. Bermudez, M. A. Martin-Delgado, and E. Solano, Phys. Rev. Lett. **99**, 123602 (2007), URL <https://link.aps.org/doi/10.1103/PhysRevLett.99.123602>.
- [62] T. M. Rusin and W. Zawadzki, Phys. Rev. D **82**, 125031 (2010), URL <https://link.aps.org/doi/10.1103/PhysRevD.82.125031>.
- [63] I. Bloch, J. Dalibard, and W. Zwerger, Rev. Mod. Phys. **80**, 885 (2008), URL <https://link.aps.org/doi/10.1103/RevModPhys.80.885>.
- [64] I. H. Deutsch and P. S. Jessen, Phys. Rev. A **57**, 1972 (1998), URL <https://link.aps.org/doi/10.1103/PhysRevA.57.1972>.
- [65] D. Jaksch, H.-J. Briegel, J. I. Cirac, C. W. Gardiner, and P. Zoller, Phys. Rev. Lett. **82**, 1975 (1999), URL <https://link.aps.org/doi/10.1103/PhysRevLett.82.1975>.
- [66] G. K. Brennen, C. M. Caves, P. S. Jessen, and I. H. Deutsch, Phys. Rev. Lett. **82**, 1060 (1999), URL <https://link.aps.org/doi/10.1103/PhysRevLett.82.1060>.
- [67] O. Mandel, M. Greiner, A. Widera, T. Rom, T. W. Hänsch, and I. Bloch, Nature **425**, 937 (2003), URL <http://dx.doi.org/10.1038/nature02008><http://10.0.4.14/nature02008>.
- [68] O. Mandel, M. Greiner, A. Widera, T. Rom, T. W. Hänsch, and I. Bloch, Phys. Rev. Lett. **91**, 10407 (2003), URL <https://link.aps.org/doi/10.1103/PhysRevLett.91.10407>.
- [69] J. C. Budich, C. Laflamme, F. Tschirsich, S. Montanero, and P. Zoller, Phys. Rev. B **92**, 245121 (2015), URL <https://link.aps.org/doi/10.1103/PhysRevB.92.245121>.
- [70] M. Aidelsburger, M. Lohse, C. Schweizer, M. Atala, J. T. Barreiro, S. Nascimbène, N. R. Cooper, I. Bloch, and N. Goldman, Nature Physics **11**, 162 (2014), URL <http://dx.doi.org/10.1038/nphys3171><http://10.0.4.14/nphys3171><https://www.nature.com/articles/nphys3171#supplementary-information>.
- [71] L. Fu and C. L. Kane, Physical Review B **74**, 1 (2006), ISSN 10980121, 0606336.
- [72] R. Shindou, Journal of the Physical Society of Japan **74**, 1214 (2005), URL <https://doi.org/10.1143/JPSJ.74.1214>.
- [73] See Supplemental Material, Sec. E for the detailed derivation.
- [74] F. Nathan and M. S. Rudner, New Journal of Physics **17**, 125014 (2015), URL <http://stacks.iop.org/1367-2630/17/i=12/a=125014>.
- [75] A. Kitaev, AIP Conference Proceedings **1134**, 22 (2009), <http://aip.scitation.org/doi/pdf/10.1063/1.3149495>, URL <http://aip.scitation.org/doi/abs/10.1063/1.3149495>.
- [76] A. P. Schnyder, S. Ryu, A. Furusaki, and A. W. W. Ludwig, Phys. Rev. B **78**, 195125 (2008), URL <https://link.aps.org/doi/10.1103/PhysRevB.78.195125>.
- [77] J. C. Y. Teo and C. L. Kane, Phys. Rev. B **82**, 115120 (2010), URL <https://link.aps.org/doi/10.1103/PhysRevB.82.115120>.
- [78] R. Roy and F. Harper, Phys. Rev. B **96**, 155118 (2017), URL <https://link.aps.org/doi/10.1103/PhysRevB.96.155118>.
- [79] T. Morimoto, H. C. Po, and A. Vishwanath, Phys. Rev. B **95**, 195155 (2017), URL <https://link.aps.org/doi/10.1103/PhysRevB.95.195155>.
- [80] See Supplemental Material, Sec. F for the detailed derivation of the correspondence.
- [81] X.-L. Qi, T. L. Hughes, and S.-C. Zhang, Phys. Rev. B **78**, 195424 (2008), URL <https://link.aps.org/doi/10.1103/PhysRevB.78.195424>.
- [82] M. Nakahara, *Geometry, topology and physics* (CRC Press, 2003).
- [83] S. Aubry and G. André, Ann. Israel Phys. Soc **3**, 18 (1980).
- [84] P. G. Harper, Proceedings of the Physical Society. Section A **68**, 874 (1955), URL <http://stacks.iop.org/0370-1298/68/i=10/a=304>.
- [85] D. Jaksch and P. Zoller, New Journal of Physics **5**, 56 (2003), URL <http://stacks.iop.org/1367-2630/5/i=1/a=356>.
- [86] N. Goldman, G. Juzelinas, P. Öhberg, and I. B. Spielman, Reports on Progress in Physics **77**, 126401 (2014), URL <http://stacks.iop.org/0034-4885/77/i=12/a=126401>.
- [87] M. Mancini, G. Pagano, G. Cappellini, L. Livi, M. Rider, J. Catani, C. Sias, P. Zoller, M. Inguscio, M. Dalmonte, et al., Science **349**, 1510 (2015), ISSN 10959203, 1502.02495, URL <http://arxiv.org/abs/1502.02495>.
- [88] B. Song, C. He, S. Zhang, E. Hajiyevev, W. Huang, X.-J. Liu, and G.-B. Jo, Phys. Rev. A **94**, 61604 (2016), URL <https://link.aps.org/doi/10.1103/PhysRevA.94.61604>.
- [89] K. Enomoto, K. Kasa, M. Kitagawa, and Y. Takahashi, Phys. Rev. Lett. **101**, 203201 (2008), URL <https://link.aps.org/doi/10.1103/PhysRevLett.101.203201>.